كلية الهندسة بشبرا
FACULTY OF ENGINEERING AT SHOUBRA
ERJ
PRINT ISSN 3009-6049
ONLINE ISSN 3009-6022

ENGINEERING RESEARCH JOURNAL (ERJ)
Volume (53) Issue (4)
October. 2024, pp:157-166
https://erjsh.journals.ekb.eg

Prediction of Shear Load Characteristics of Dissimilar Friction Stir Spot Welded Joints using Neural Network Model

Amr Mohamed Hanafy[1] *,Ahmed Gaafer [2], Sayed Hamza Mansour[2], Hamed A. Abdel-Aleem[3]
[1]Higher technological institute
[2] Department of Mechanical Engineering, Faculty of Engineering at Shoubra, Benha University, Cairo, Egypt.
[3]Welding Technology and NDT Department, Central Metallurgical Research and Development Institute (CMRDI), Cairo, Egypt.
* Corresponding Author.
E-mail: hamedaa@gmail.com, ahmed.marzouk@feng.bu.edu.eg, amr.hanafy@hti.edu.eg, alsayed.abdelhady@feng.bu.edu.eg

Abstract: An artificial neural network (ANN) system was developed and implemented for analyzing and simulating the process parameters concerning -aluminum alloy 6061 and pure copper - dissimilar welded joints for their mechanical properties. In the present study, 2.2 mm thick Aluminum alloy 6061 and 1.4 mm thick pure copper are welded using the friction stir spot welding process. The process parameters involved in welding are the tool rotation speed, plunge depth, and dwelling time. There exists an optimized level of the parameters of friction stir spot welding (FSSW) for the highest shear load of AA 6061 and pure copper lap-welded joints, predicted as 20 seconds with a plunge depth of 0.2 mm at 2000 rpm. The shear load increases with a further increase in the plunge depth for a 15 seconds dwell time and 2000 rpm. The network of 10 neurons achieves the best performance with the highest validation and test correlation coefficients, whereas the network of 20 neurons may be overfitting or underfitting, as suggested by its lower training correlation coefficient.

Keywords : Friction stir spot welding, AA 6061, Pure Copper, ANOVA.

1. INTRODUCTION

Friction stir spot welding (FSSW) has become a popular alternative process recently for spot welding technologies [1,2]. FSSW has received many industries' attention, of which the automotive industry is the most [3,4]. FSSW is a variant of friction stir welding and has many advantages in comparison to other techniques of welding. It has been widely recognized for its economic benefits, particularly its lower investment and maintenance costs when compared to other welding techniques, as noted in several studies [5-7]. Welding dissimilar metals means joining two different metals, where a transition layer will be made having different properties and microstructure than the base metal. Compared with welding the same material, welding dissimilar metals has a more complex welding mechanism and operation technology [8].

Aluminum alloys and commercial copper alloys are extensively used in the manufacturing of aircraft and automobiles due to their excellent strength, high corrosion resistance, superior formability, and ease of machinability [9-13]. In the aircraft industry, aluminum alloys and pure copper alloys are used for electrical components and heat exchangers, resulting in improved electrical conduction and heat dispersion. In the automobile industry, battery systems and cooling solutions are enhanced, leading to better performance in power electronics and PCBs, where heat management is more effectively managed. In renewable energy, solar panels and wind turbines are optimized, allowing for efficient energy transfer at a reduced weight. These are the applications where aluminum bonding to copper is critical for enhancing performance and efficiency across sectors. However, these alloys also are a significant problem in design and welding because the melting points of aluminum and copper are very different, which reduces the effective use of the conventional fusion welding processes [14]. Consequently, these dissimilar joints are riveted. FSSW has also been used extensively in the fabrication of body panels in automobiles and is efficient for welding aluminum and copper in aluminum car bodies [15-18].

Several artificial intelligence (AI) applications and the development of models in artificial neural network (ANN) for engineering areas have focused on developing many

studies in the fields of prediction, tracking, and control of manufacturing processes [19]. Dehabadi et al. [20] reported that two feed-forward backpropagation artificial neural network (ANN) techniques were employed to model and predict the Vickers microhardness of AA6061 friction-stir welded plates. The mean absolute percentage error (MAPE) during the training process for both ANN was less than 4.83%, indicating that the models' predictions exhibited an acceptable deviation from the actual microhardness values. Bîrsan et al. [21] concluded that a trained neural network can be used to predict the values of temperatures and stresses under specified conditions of pin penetration, rotation speed, and holding time.

2. EXPERIMENTAL WORK

2.1 Material and Methodology

In this Investigation, the dissimilar materials that joined by FSSW are the aluminum alloy 6061 and pure copper. The chemical composition of AA 6061 alloy and pure copper plates been given in Table 1. The shape of the rotational tool used in the investigations, having a flat shoulder and cylindrical threaded probe, is fabricated from H13 hot-worked tool steel, as shown in Fig. 1. The tool has a cylindrical shoulder with a diameter of 10 mm and a threaded probe with a diameter of 4 mm. The input parameters of the system include the plunge depth, dwell time, and rotation speed as shown in Table 2. The mechanical properties of AA 6061, pure copper plates and H13 material are listed in Table 3. Welding experiments with process parameters is shown in Table 4. The welding experiments are conducted via Harvad CNC Automatic Machine at different welding parameters. Vertical plunge rate of 150 mm/min is applied during the insertion of the tool in the overlapped plates. The Aluminum plate is placed on the upper side and the copper plate is placed on the bottom side of the process due to lower thermal conductivity of Aluminum plate that produced sufficient heat for better mixing of the joint [22-23]. The dissimilar plates are prepared to the welding process by fixing plate made from steel 37. The plates are supported by two pressure bars to prevent lifting the lap plates. The configuration of FSSW process consists of fixtures, AA 6061 plates, pure copper plates, fixing bolts, pressure bars and rotational tool as illustrated in Fig. 2. The weld lap shear load tests are performed on a SHIMADZU UH-F1000KNI-up to 1000KN test load- universal testing machine. The tensile shear experiments are performed using specimens of the given dimensions according to ISO 14273:2016 [24], as shown in Fig. 3. For thicknesses ratio of the two sheets exceeds 1.4mm, shim plates must be used to clamp the test specimen securely in the grips of the tensile shear testing machine as shown in Fig. 4. Tests are carried out at a constant cross head of 1 mm/min. The tensile shear force measured is the average value obtained from tensile tests conducted on three specimens for each welding condition.

TABLE 1. AA 6061 and Pure copper chemical compositions.

Wt%	**Cu**	**Ag**	**As**	**Sb**	**S**	**P**	**Fe**	**Ni**	**Mn**
Pure copper	99.95	0.001	0.002	0.006	0.002	0.001	0.005	0.002	0.001
Wt%	**Si**	**Fe**	**Cu**	**Mn**	**Mg**	**Cr**	**Zn**	**Ti**	**Al**
AA 6061	0.69	0.6	0.28	0.006	1.03	0.15	0.001>	0.014	Remaining

TABLE 2. Welding process parameters.

Process parameter	**Level 1**	**Level 2**	**Level 3**
Rotational Speed ω (rpm)	1800	2000	2200
Dwell Time T (sec)	10	15	20
Plunge Depth PD (mm)	0	0.1	0.2

TABLE 3. Mechanical properties of AA 6061, pure Copper plates and H13 material.

Material	AA 6061	Pure Copper	H13 Tool Steel
Tensile strength, Mpa	260	315	1955
Yield strength, MPa	206	280	1560
Hardness	67 Hv	42 Hv	653 Hv

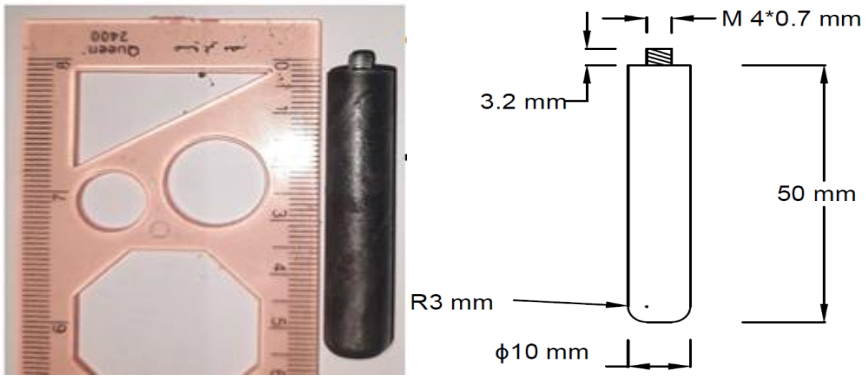

a) b)

FIGURE 1. Rotational tool dimensions (a) schematic drawing (b) machined tool.

TABLE 4. Welding experiments with process parameters.

Specimen no	Rotational speed (rpm)	Dwell Time (sec)	Plunge Depth (mm)
1	1800	10	0
2	1800	15	0
3	1800	20	0
4	1800	10	0.1
5	1800	15	0.1
6	1800	20	0.1
7	2000	10	0
8	2000	15	0.1
9	2000	20	0.2
10	2000	10	0.1
11	2000	15	0.2
12	2000	20	0
13	2200	10	0.1
14	2200	15	0.1
15	2200	20	0.1
16	2200	10	0.2
17	2200	15	0.2
18	2200	20	0.2

FIGURE 2. Friction stir spot welding parts.
a) Fixtures b) AA 6061 plate c) Pure copper plate d) Bolt e) Pressure Bar f) Rotational tool.

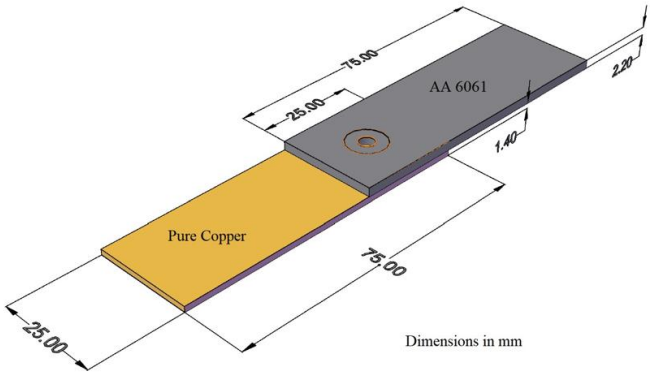

FIG 3. Tensile shear specimen.

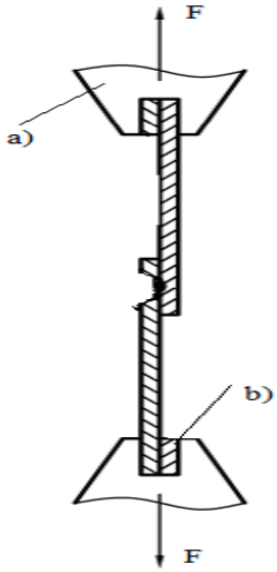

FIG 4. Tensile shear test configuration a) grip b) shim.

2.2 Back Propagation Neural Network (BPN)

Neural systems are computational models that mimic the functions of biological neural networks, comprising neurons, and are utilized for various complex tasks across different applications. These systems include three layers: the input layer, the hidden layer, and the output layer. The input layer handles process parameters such as rotational speed, plunge depth, and dwell time. According to Fig 5, the hidden layer contains 5, 10, or 20 neurons. The output layer represents the tensile shear force of the welded joints. This model operates using feed-forward back propagation neural networks.

3. RESULTS

3.1 Tensile Shear Force Results

AA 6061 and pure copper plates have been successfully joined using spot lap welding. Some examples of these welds are shown in Fig. 5. The visual inspection of welded specimens' area is presented. The lack of penetration defect observed in specimen condition 4 - number 3 (A4-3) and condition 4- number 6 (A4-6) is attributed to low plunge depth caused by the vibrations of the rotational tool in the CNC machine. The excess flashes occurred due to excessive heat generation because of the higher rotational speed. The top view of the spot-welded joints reveals that the extruded material flashing to the sides of the shoulder projection is nearly identical. Circular indentations caused by the shoulder projection are observed under various applied parameters [25]. Excessive flash is minimized by the meticulous selection of FSSW parameters, informed by insights from previous studies [26]. The tensile-shear force values of the lap joints are influenced by changes in process parameters. The maximum tensile shear force, measured at 4.13 KN, is achieved with a rotational speed of 2000 rpm, a plunge depth of 0.2 mm, and a dwell time of 20 seconds. This is because of the improved mixing between aluminum and copper. The rotational speed of 2000 rpm contributes to better heat input, while the dwell time allows sufficient time for stirring the joint.

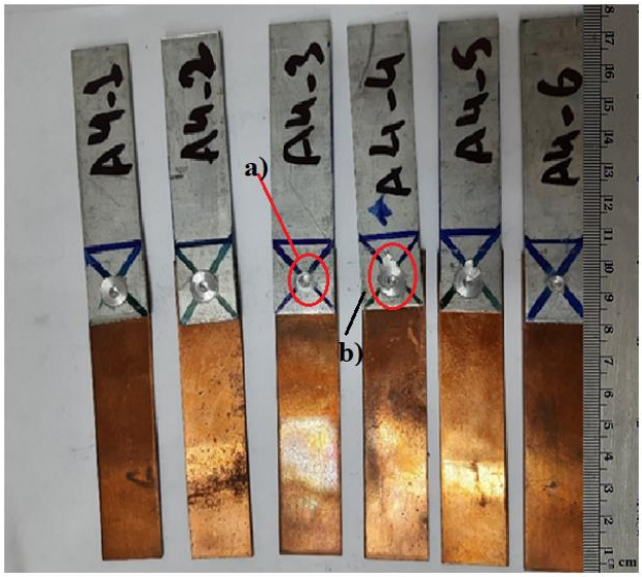

FIG 5. Visual inspection of weld specimens at 1800 rotational speed , 10 seconds dwell time and 0.1mm plunge depth with a) lack of penetration b) excess flashes.

Contrarily, the minimum tensile shear force, 2.01 KN, is obtained with a tool rotational speed of 2200 rpm, a plunge depth of 0.1 mm, and a dwell time of 15 seconds. The combination of high rotational speed and shallow plunge depth likely results in insufficient heat generation and inadequate material mixing, leading to a weld with low shear strength [27]. Garg et al. [28] reported that the lap shear force of Cu-AA6061 joints decreased with increasing test temperature when no preheating was used. However, for joints that underwent preheating, the lap shear force increased from 1.63 KN at a 25°C test temperature to 2 KN at 50°C. It then decreased to 1.8 KN at a 100°C test temperature.

It is observed that at 1800 rpm and zero plunge depth, the tensile shear force initially increases with dwell time from 10 to 15 seconds, then decreases when the dwell time reaches 20 seconds, as illustrated in Fig. 6. This is because the longer dwell time allows for better heat generation and material mixing, leading to a stronger weld. However, when the dwell time extends to 20 seconds, the tensile shear force decreases. The extended dwell time may lead to overheating and potential defects such as grain coarsening or excessive softening of the material, which can weaken the weld. Chu et al. [29] reported that the material flow behavior becomes unstable at shorter dwelling times. The shear force varies with changes in rotational speed. As rotational speed increases from 1800 rpm to 2000 rpm, the shear force rises from 2.4 KN to 2.98 KN. This increase is due to improved heat generation and material mixing, leading to a stronger weld. However, when the rotational speed is further increased to 2200 rpm, the shear load decreases to 2.7 KN. This reduction is likely caused by excessive heat, which can result in defects such as voids or material degradation, thereby weakening the weld. This trend is depicted in Fig. 7. Additionally, it is found that the shear lap force increases as the plunge depth values rise. The optimum tensile shear force is shown to be the highest in Fig. 8. Increasing the plunge depth enhances the downward force, thereby improving heat input and promoting better material flow between aluminum and copper. This results in improved mixing within the welded joint and an increase in the shear load of the joint. Piccini et al. [30] investigated the effect of plunging depth during the FSSW process and the impact of changing the position of the alloys in superimposed joints when welding AA5052 and AA6063 sheet specimens. They found that the fracture load increased with greater tool plunging depth for both configurations.

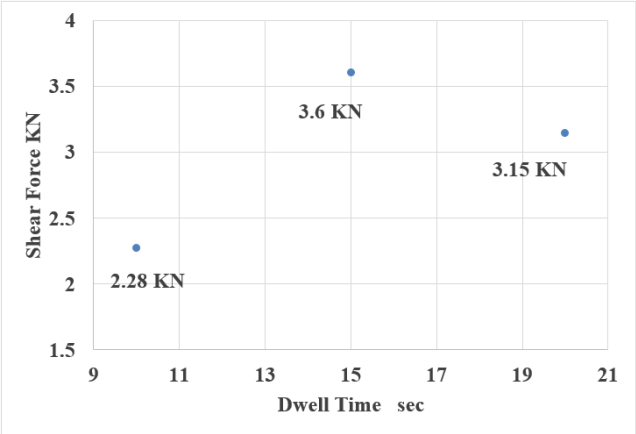

FIG 6. Effect of dwell time on shear force at 1800 rpm- zero mm plunge depth.

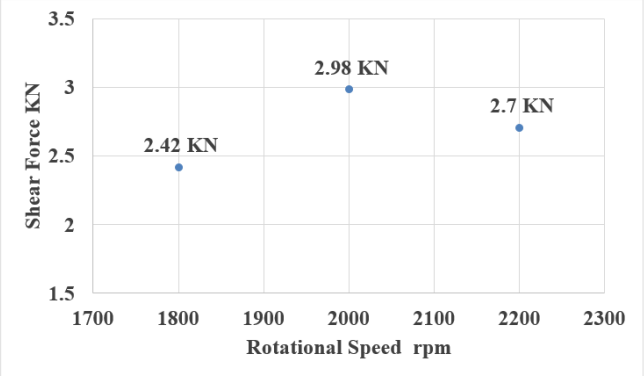

FIG 7. Effect of rotational speed on shear force at 10 seconds dwell time- 0.1 mm plunge depth.

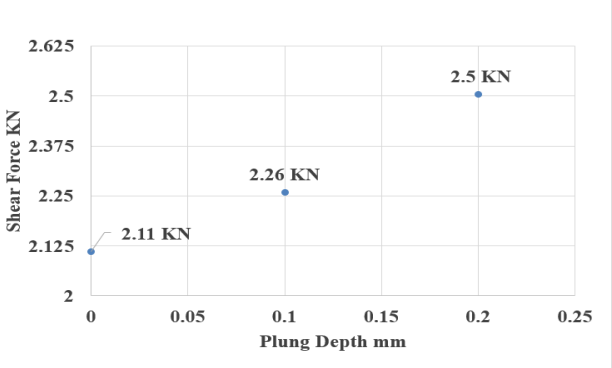

FIG 8. Effect of plunge depth on shear force at 2000 Rpm- 15 seconds dwell time.

3.2 Training the Network

In the training process of artificial neural networks (ANN), various parameters were assessed. For all cases in this study, feed-forward artificial neural networks are utilized in the models. The process included database collection, analysis of the data, training of the neural network, testing of the trained network, and using the trained NN for simulation and prediction. The MATLAB platform is employed for training and testing the ANN. During the training phase, an increased number of neurons in the hidden layer are used to accurately define the output. Training of the network: It uses the Levenberg-Marquardt (LM) back-propagation algorithm. The tan-sigmoid activation functions reach the input as well as the output of the hidden layers in this study. Kulekci et al. [31] reported that the dataset of study the neural network model provides predictions of tensile shear strength that are closer to the experimental values compared to those obtained through regression analysis. Table 5 indicates the tensile shear force between the measured and predicted tensile shear force results of 5, 10, and 20 neurons, along with the associated error percentages as shown in Fig. 9. There are 18 samples used in neural system test data. Next, through the hidden layers, 5, 10, and 20 neurons are implemented in the neural system. It consists of three original data splits, and training, validation, and test data are 60%-20%-20%, respectively.

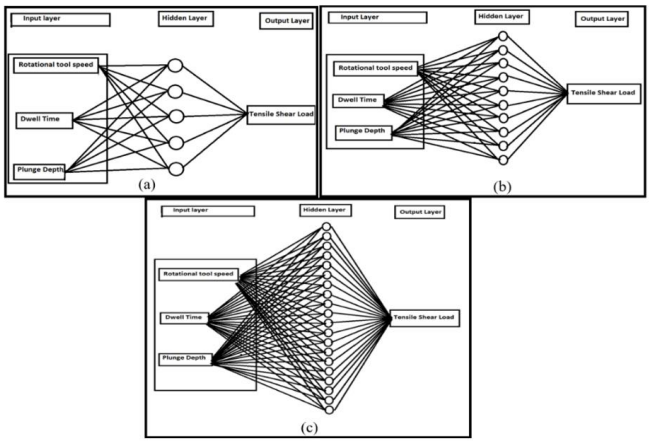

FIG 9. Developed neural networks with a) 5 b) 10 c) 20 neurons of hidden layers.

Inputs and outputs have been normalized in the range of 0–1. The formulation of the hidden and output layers using the 'Tan-sigmoid' transfer function is employed to predict the tensile shear force values and is responsible for connecting the input and output nodes within the network. Equation (1) shows the Tan-sigmoid transfer Function [32].

Equation (1) :

$$F(x) = \frac{2}{1+e^{-2x}} - 1 \quad (1)$$

After successfully training the network, it was subjected to testing using established test data. Statistical techniques were employed to assess the outcomes generated by the network. The occurrence of errors is a common phenomenon during the training of networks, hence the determination of the Coefficient of Correlation (R) and the mean square error.

TABLE 5. Predicted values of neural networks shear load with welding process parameters.

Rotational speed (rpm)	Dwell Time (sec)	Plunge Depth (mm)	Shear Force (KN)									
			Measured				5 neurons		10 neurons		20 neurons	
			1	2	3	average	value	Error%	value	Error%	value	Error%
1800	10	0	1.29	3.06	2.48	2.28	2.5245	10.72	2.3112	1.37	2.2679	-0.53
1800	15	0	3.26	3.33	4.23	3.60	3.5917	-0.23	3.5886	-0.32	3.9558	9.88
1800	20	0	3.01	3.01	3.42	3.15	3.095	-1.75	3.1476	-0.08	3.1702	0.64
1800	10	0.1	3.12	2.06	2.08	2.42	2.4562	1.50	2.3792	-1.69	3.8892	60.71
1800	15	0.1	2.16	2.09	3.03	2.43	2.4542	1.00	2.4246	-0.22	2.4257	-0.18
1800	20	0.1	3.21	3.15	2.08	2.81	2.8719	2.20	2.8107	0.02	2.8111	0.04
2000	10	0	1.73	3.32	2.5	2.52	2.4572	-2.49	2.5093	-0.42	2.5212	0.05
2000	15	0.1	1.84	2.74	2.19	2.26	2.2569	-0.14	2.2547	-0.23	2.0176	-10.73
2000	20	0.2	4.17	4.04	4.18	4.13	3.6995	-10.42	2.9289	-29.08	4.1264	-0.09
2000	10	0.1	2.56	2.68	3.71	2.98	2.4538	-17.66	2.3284	-21.87	2.011	-32.52
2000	15	0.2	2.26	2.42	2.83	2.50	2.4997	-0.01	2.3927	-4.29	2.5138	0.55
2000	20	0	1.71	2.96	3.83	2.84	2.8237	-0.57	2.8301	-0.35	2.0104	-29.21
2200	10	0.1	2.16	4.18	1.77	2.70	2.8955	7.24	2.6772	-0.84	2.0318	-24.75
2200	15	0.1	1.79	1.94	2.29	2.01	2.0204	0.52	2.0906	4.01	2.2641	12.64
2200	20	0.1	3.78	3.68	3.87	3.77	3.7733	0.09	3.6169	-4.06	3.6789	-2.42
2200	10	0.2	3.78	1.09	2.52	2.46	2.0108	-18.26	2.522	2.52	3.7776	53.56
2200	15	0.2	3.13	2.63	3.37	3.04	2.012	-33.82	3.0601	0.66	2.9964	-1.43
2200	20	0.2	2.56	2.39	2.10	2.35	2.3484	-0.07	2.9129	23.95	4.127	75.62

3.3 Regression Analysis and Performance Curve

Figure 10a shows the regression analysis for a hidden layer network with 5 neurons. The training data demonstrates an excellent fit (R=0.99795) with the data points closely following the regression line. The validation data also shows a reasonable fit (R=0.85594), indicating good performance. However, the test data reveals a poor fit (R=-0.68559), which may suggest overfitting, where the model performs well on training data but fails to generalize to new data. Overall, the model's performance is decent (R=0.85033), but the disparity between the training and test results highlights the need for further improvement to avoid overfitting and ensure better generalization. Figure 10b shows the regression analysis for a hidden layer network with 10

neurons. The training data shows a moderate fit (R=0.84057), while the validation data demonstrates an excellent fit (R=0.99463), indicating strong generalization. The test data also exhibits a good fit (R=0.91836), confirming the model's effectiveness on new data. However, the overall R value of 0.78637 suggests some inconsistencies across the entire dataset, indicating potential areas for further model refinement. Figure 10c shows the regression analysis for a hidden layer network with 20 neurons. The training data shows a weak fit (R=0.2849), while the validation data exhibits a strong fit (R=0.92197), indicating good generalization. However, the test data shows a poor fit (R=-0.60126), suggesting overfitting. The overall R value of 0.47653 indicates inconsistencies across the dataset, signaling the need for model refinement.

The network with 10 neurons shows the best overall performance, exhibiting the highest validation and test correlation coefficients, while the network with 20 neurons indicates potential overfitting or underfitting issues, as evidenced by the lower training correlation coefficient.

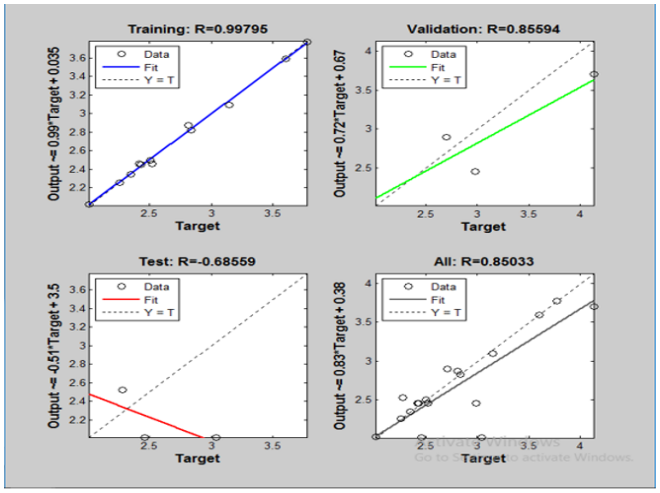

a)

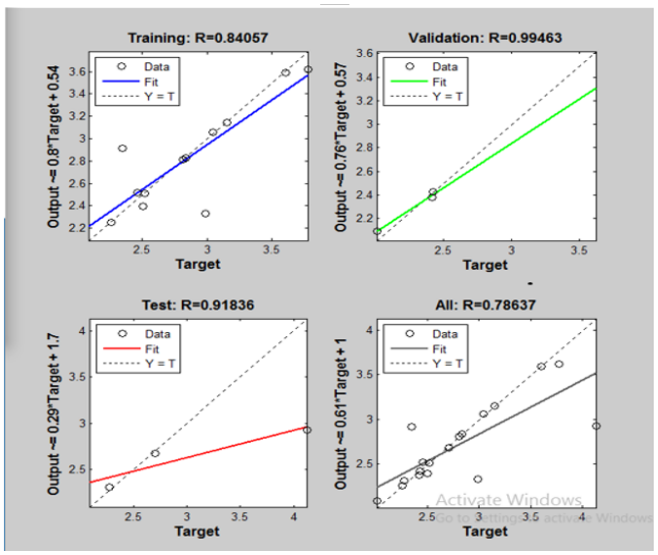

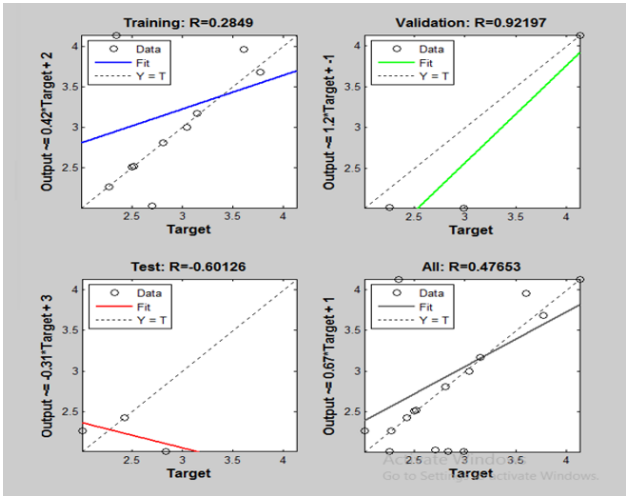

c)

FIG10. Regression analysis for a) 5, b) 10 and c) 20 neurons hidden layer network.

Figure 11a shows the performance curve for a network with 5 neurons in the hidden layer. The best validation performance is achieved at epoch 8 with an (mean squared error) MSE of 0.16662. Despite a steady decrease in training error, the validation and test errors remain relatively high, indicating possible underfitting due to the limited number of neurons. Figure 11b shows the performance curve for a network with 10 neurons, where the MSE curve over just 4 epochs reveals a rapid decrease in training error, with both validation and test errors stabilizing quickly. This results in an exceptionally low validation MSE of 0.0026141 at epoch 0, indicating highly effective training. Figure 11c illustrates the performance curve for a network with 20 neurons. The best validation performance is recorded at epoch 0 with an MSE of 0.33446. The significant gap between the training error and the validation/test errors indicates overfitting, where the model fails to generalize well to new data.

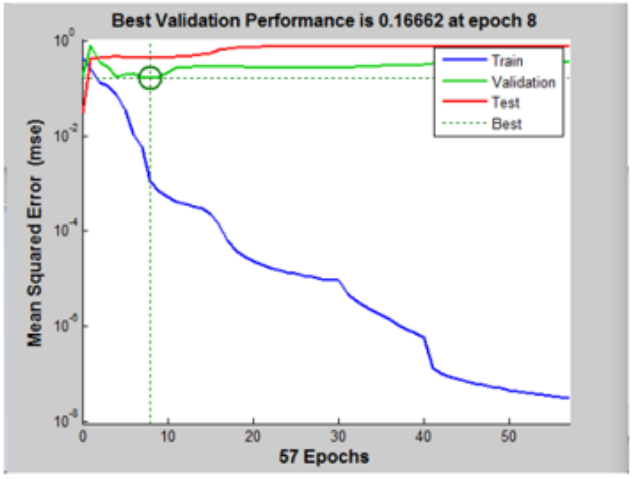

a)

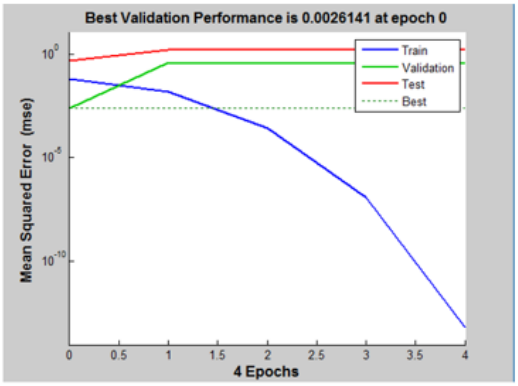

b)

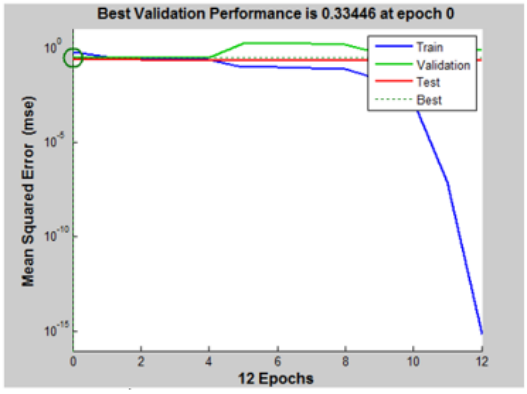

C)

FIG 11. Performance curves for a) 5, b) 10 and c) 20 neurons hidden layer.

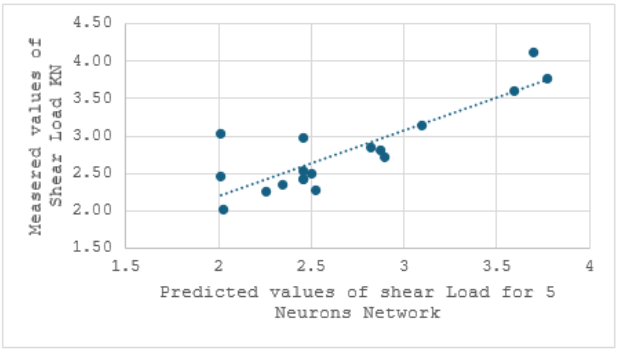

a)

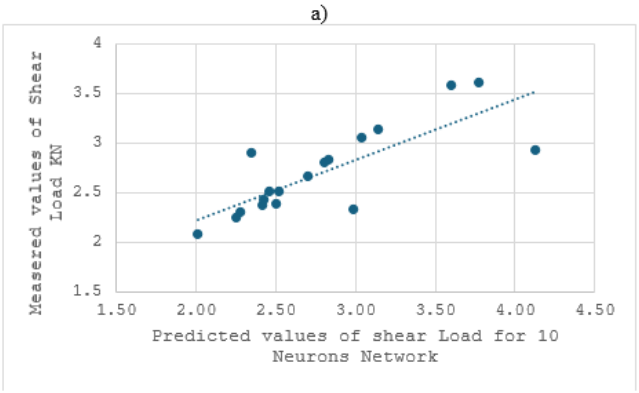

b)

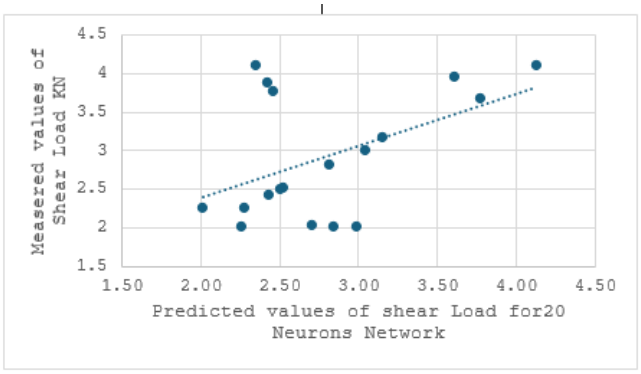

c)

FIG 12. Comparison between experimental and predicted values of shear load at a) 5 neurons, b) 10 neurons and c) 20 neurons of hidden layer

Figure 12a shows a comparison between experimental and predicted shear load values using 5 neurons hidden layer. The scatter plot reveals a reasonable correlation, with the predicted values generally following the trend of the measured values, although some deviations are observed, particularly at higher shear loads. Figure 12b illustrates a comparison between the experimentally measured shear load values and those predicted by the model with 10 neurons hidden layer. The correlation is stronger, with predicted values closely matching the measured ones, indicating a better fit and improved model performance. The regression line aligns more closely with the ideal fit, suggesting that this configuration better captures the underlying relationship. Figure 12(c) presents the comparison between experimental and predicted shear load values using 20 neurons hidden layer. In this case, the correlation is less consistent, with greater variability and more significant deviations from the measured values, especially at lower shear loads. The regression line indicates a weaker fit, which might suggest issues like overfitting or underfitting.

The network with 10 neurons shows the best performance, achieving the highest validation and test correlation coefficients, while the 20-neuron network exhibits potential overfitting or underfitting, as reflected by its lower training correlation coefficient. Jo et al. [33] concluded that FSSW of 1.6-mm thick AA6061-T6 plates resulted in an experimental tensile shear force of 4.0 kN, with a predicted value of 4.147 kN, leading to a 3.675% error. The hardness showed a 3.197% error, with an experimental value of 62 Hv and a predicted value of 60.018 Hv. Abdullah et al. [34] reported that a mean relative error (MRE) of approximately 3.42% was observed in the developed ANN model for predicting the tensile shear load (TSL) of AA7020-T6 lap joints. Nugroho et al. [35] developed an ANN network that proved to be the most accurate model for predicting the maximum tensile shear load compared to other models, with

an MSE of 0.00918 and an average error of 6.99%.

4. CONCLUSIONS

In this study, AA6061 and pure copper plates were welded using friction stir spot welding at varying speeds (1800, 2000, 2200 rpm), dwell times (10, 15, 20 seconds), and plunge depths (0, 0.1, 0.2 mm). Tensile-shear tests were performed to determine the optimal shear force of the lap joints. An ANN model was developed to train, test and predict the results.

Based on the obtained results, the following conclusions can be outlined:

1- The highest shear load for AA 6061 and pure copper lap joints was achieved at 2000 rpm, 20 seconds dwell time, and a 0.2 mm plunge depth due to better heat input and sufficient mixing between aluminum and copper.

2- At 2000 rpm and a 15 second dwell time, the shear load increased from 2.11 KN to 2.5 KN as the plunge depth increased from 0 to 0.2 mm. The greater plunge depth enhanced downward force and heat input, resulting in a higher shear load.

3- At 1800 rpm with zero plunge depth, the shear load increased to 3.6 KN at 15 seconds but dropped to 3.14 KN at 20 seconds, as prolonged dwell time caused overheating and weld weakening.

4- The network with 10 neurons provided the best fit for predicting shear loads, while 5 neurons gave a reasonable fit with minor deviations. However, using 20 neurons led to overfitting or underfitting, reducing prediction accuracy. Increasing neurons improved performance only up to a certain point.

REFERENCES

[1]. M. Newishy, M. Jaskari, A. Järvenpää, H. Fujii, and H. Abdel-Aleem, "Friction Stir Welding of Dissimilar Al 6061-T6 to AISI 316 Stainless Steel: Microstructure and Mechanical Properties," Materials, vol. 16, no. 11, 2023, p.1-21.

[2]. M. H. Fahmy, H. Abdel-Aleem, N. A. Abdel-Elraheem, M. R. El-Kousy, "Friction Stir Spot Welding of AA2024-T3 with Modified Refill Technique," Key Engineering Materials, vol. 835, 2020, pp. 274-287.

[3]. T. Shibayanagi, M. K. Mizushima, S. Yoshikawa, K. Ikeuchi, "Friction Stir Spot Welding of Pure Aluminum Sheet in View of High Temperature Deformation," Transactions of Joining and Welding Research Institute, vol. 40, no. 2, 2011, pp. 1-5.

[4]. M. S. Mohd Isa, K. Moghadasi, M. A. Ariffin, S. Raja, M. R. Muhamad, F. Yusof, M. F. Jamaludin, N. Yusoff, and M. S. Ab Karim, "Recent Research Progress in Friction Stir Welding Of Aluminium and Copper Dissimilar Joint: A Review," Journal of Materials Research and Technology, vol. 15, 2021, pp. 2735-2780.

[5]. Yang Xu, L. Ke, S. Ouyang, Y. Mao, P. Niu, "Precipitation Behavior of Intermetallic Compounds and Their Effect on Mechanical Properties of Thick Plate Friction Stir Welded Al/Mg Joint," Journal of Manufacturing Processes, vol. 64, 2021, pp. 1059-1069.

[6]. M. Ragab, H. Liu, H. Abdel-Aleem, M. M. E. S. Seleman, M. M. Z. Ahmed, G. Mehboob, "Numerical and Experimental Study of Underwater Friction Stir Welding Of 1Cr11Ni2W2MoV Heat-Resistant Stainless Steel," Journal of Materials Research and Technology, vol. 29, March–April 2024, pp. 130-148.

[7]. V. Balasubramanian, "Relationship Between Base Metal Properties and Friction Stir Welding Process Parameters," Materials Science and Engineering: A, vol. 480, no. 1–2, 2008, pp. 397-403.

[8]. R. Karthikeyan, V. Balasubramanian, "Predictions of The Optimized Friction Stir Spot Welding Process Parameters for Joining AA2024 Aluminum Alloy using RSM," The International Journal of Advanced Manufacturing Technology, vol. 51, no.1, 2010, pp. 173-183.

[9]. J. You, Y. Zhao, C. Dong, & Y. Su, "Improving The Microstructure And Mechanical Properties of Al-Cu Dissimilar Joints by Ultrasonic Dynamic-Stationary Shoulder Friction Stir Welding," Journal of Materials Processing Technology, vol. 311, 2023, pp.1-20.

[10]. O. Mypati, S. K. Pal, S. K. Pal, P. Srirangam "An Investigation of Mechanical and Electrical Properties of Friction Stir Welded Al and Cu Busbar for Battery Pack Applications," Materials Chemistry and Physics, vol. 287, 2022, p. 1-31.

[11]. C. Connolly, "Friction spot joining in aluminum car bodies," Industrial Robot, vol. 34, no. 1, 2007, pp. 17-20.

[12]. R. Khajeh, H. R. Jafarian, R. Jabraeili, A. R. Eivani, S. H. Seyedein, N. Park, A. Heidarzadeh, "Strength-Ductility Synergic Enhancement in Friction Stir Welded AA2024 Alloy and Copper Joints: Unravelling the Role of Zn Interlayer's Thickness," Journal of Materials Research and Technology, vol. 16, 2022, pp. 251-262.

[13]. H. Abdel-Aleem, S. A. Khodir, "Evaluation of Ultrasonic Dissimilar Welds by Ultrasonic Testing Immersion Method C-Scope Mode," Academic Journal of Manufacturing Engineering, vol. 15, no. 4, 2017, pp.1864-1874.

[14]. S. A. Khodir, M. M. Z. Ahmed, E. Ahmed, S. M. R. Mohamed, H. Abdel-Aleem, "Effect of Intermetallic Compound Phases on The Mechanical Properties of The Dissimilar Al/Cu Friction Stir Welded Joints," Journal of Materials Engineering and Performance, vol. 25, 2016, pp. 4637–4648.

[15]. W.B. Lee, S.B. Jung, "Void Free Friction Stir Weld Zone of The Dissimilar 6061 Aluminum and Copper Joint by Shifting the Tool Insertion Location," Materials Research Innovations, vol. 8, 2004, pp. 93–96.

[16]. M. Morsy, H. Abdel-Aleem, E. El-Kashif, "Dissimilar Friction Stir Spot Welding of Aluminum, Steel, And Brass Alloys," Journal of Engineering and Applied Science, vol. 57, no. 2, 2010, pp. 149-165.

[17]. M. M. Z. Ahmed, E. Ahmed, S. M. R. Mohamed, and H. Abdel-Aleem, "Friction Stir Spot Welding of Aluminum and Copper: A Review," Materials, vol. 13, no. 1, 2020, pp. 156-182.

[18]. M. S. M. Isa, M. R. Muhamad, F. Yusof, N. Yusoff, Z. Brytan, T. Suga, Y. Morisada, and H. Fujii, "Improved Mechanical and Electrical Properties of Copper-Aluminum Joints with Highly Aligned Graphene Reinforcement Via Friction Stir Spot Welding," Journal of Materials Research and Technology, vol. 24, 2023, pp. 9203-9215.

[19]. A. Bezazi, S. G. Pierce, K. Worden, "Fatigue Life Prediction of Sandwich Composite Materials Under Flexural Tests Using a Bayesian Trained Artificial Neural Network," International Journal of Fatigue, vol. 29, no. 4, 2007, pp. 738-747.

[20]. V. M. Dehabadi, S. Ghorbanpour, G. Azimi, "Application of Artificial Neural Network to Predict Vickers Microhardness of AA6061 Friction Stir Welded Sheets," Journal of Central South University, vol. 23, 2016, pp. 2146-2155.

[21]. D. C. Bîrsan, V. Păunoiu, and V. G. Teodor, "Neural Networks Applied for Predictive Parameters Analysis of The Refill Friction Stir Spot Welding Process Of 6061-T6 Aluminum Alloy Plates," Materials, vol. 16, no. 15, 2023, pp.1-21

[22]. A.N. Colmenero, M.S. Orozco, E.J. Macias, J.B. Fernandez, J.C.S.D. Muro, H.C. Fals, and A.S. Roca, " Optimization of Friction Stir Spot Welding Process Parameters for Al-Cu Dissimilar Joints Using the Energy of The Vibration Signals," International Journal of Advanced Manufacturing Technology, vol. 100, 2019, pp. 2795-2802.

[23]. M. Akbari, R. Abdi Behnagh, and A. Dadvand, "Effect of Materials Position on Friction Stir Lap Welding of Al to Cu," Science and Technology of Welding and Joining, vol. 17, 2012, pp. 581-588.

[24]. ISO. "Resistance Welding - Destructive Testing of Welds - Specimen Dimensions and Procedure for Tensile Shear Testing Resistance Spot and Embossed Projection Welds." ISO 14273:2016. International Organization for Standardization, Geneva, Switzerland, 2016. pp 1-8.

[25]. H. Aydın, O. Tunçel, M. Tutar, and A. Bayram, "Effect of Tool Pin Profile on The Hook Geometry and Mechanical Properties of a Friction Stir Spot Welded AA6082-T6 Aluminum Alloy," Transactions of the Canadian Society for Mechanical Engineering, vol. 45, 2021, pp. 233-248.

[26]. M.M.Z. Ahmed, M.M. El-Sayed Seleman, E. Ahmed, H.A. Reyad, K. Touileb, and I. Albaijan, "Friction Stir Spot Welding of Different Thickness Sheets of Aluminum Alloy AA6082-T6," Materials, vol. 15, 2022, p. 2971-2991.

[27]. H. M. Rao, W. Yuan, H. Badarinarayan, "Effect of Process Parameters on Mechanical Properties of Friction Stir Spot Welded Aluminum Alloys," Materials and Design, vol. 30, no. 10, December 2009, pp. 4293-4301.

[28]. A. Garg and A. Bhattacharya, "Friction Stir Spot Welding of AA6061-T6 And Cu with Preheating: Strength and Failure Behavior at Different Test Temperatures," The International Journal of Advanced Manufacturing Technology, vol. 108, 2020, pp. 2153-2165.

[29]. Q. Chu, X. W. Yang, W. Y. Li, Y. Zhang, T. Lu, A. Vairis, W. B. Wang, "On Visualizing Material Flow and Precipitate Evolution During Probeless Friction Stir Spot Welding of An Al-Li Alloy," Materials Characterization, vol. 144, 2018, pp. 336-344.

[30]. J.M. Piccini and H.G. Svoboda, "Effect of The Tool Penetration Depth in Friction Stir Spot Welding (FSSW) Of Dissimilar Aluminum Alloys," Procedia Materials Science, vol. 8, 2015, pp. 868-877.

[31]. M.K. Kulekci, U. Esme, O. Er, and Y. Kazançoğlu, "Modeling and Prediction of Weld Shear Strength in Friction Stir Spot Welding Using Design of Experiments And Neural Network," Materials Science and Engineering Technology, vol. 42, no. 11, 2011, pp.990-995.

[32]. Jaan, Kiusalaas. "Numerical Methods in Engineering with Matlab." Cambridge University Press, New York, USA, 2009, pp 1-435.

[33]. D. S. Jo, P. Kahhal, and J. H. Kim, "Optimization of Friction Stir Spot Welding Process Using Bonding Criterion and Artificial Neural Network," Materials, vol. 16, no. 10, pp. 3757, 2023.

[34]. I. Abdullah, S.S. Mohammed, and S.A. Abdallah, "Artificial Neural Network Modelling of The Mechanical Characteristics of Friction Stir Welded AA7020-T6 Aluminum Alloy," Engineering Research Journal (ERJ), vol. 1, no. 46, October 2020, pp. 6-10.

[35]. A.A.D. Nugroho, E. Sofyan, D. Hendriana, E.A. Wibowo, F. Widiatmoko, and S.D. Panggayuh, "Application of An Artificial Neural Network Model to Predict Parameter of Friction Stir Spot Welding on Aluminum Sheet," Proceeding of Conference on Management and Engineering in Industry, Mechatronics, vol. 3, no. 1, August 2021, pp. 207-211.